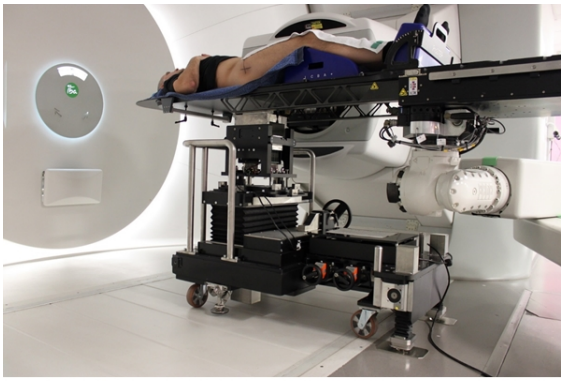

Fig 1: PGI slit camera, positioned under the patient table using a floor-fixed docking station. The camera position can be shifted in beam direction to be centered to the optimal field of view. The absolute camera position relative to room isocenter was calibrated and quality assured using both, the orthogonal x-ray system as well as beam measurements in a homogenous target.

Results

The accuracy and precision for global PGI range verification (averaging over multiple spots) was determined to be 0.7 mm (2σ) and 1.3 mm (2σ), respectively. The precision is limited by remaining uncertainties in image registration and positioning reproducibility (1.1 mm, 2σ). Hence, the absolute verification uncertainty of the cumulative mean shift (for 9 monitored fractions) is 0.8 mm (2σ), which is smaller than the range prediction uncertainty for deep-seated tumors (about 10 mm for prostate treatments). The comparison of the PGI-measured and predicted spot-wise ranges for in total 12000 PBS spots from the 9 analyzed fractions resulted in an range prediction offset of 0.6 mm, 1.3 mm and 4.4 mm, for the DirectSPR, Adapt-HLUT and Std-HLUT approaches, respectively.

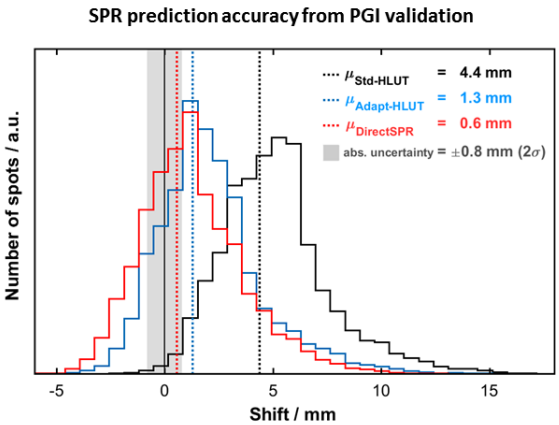

Fig 2: Histogram of range shifts, obtained with each of the respective range prediction models. The data comprises the shifts of about 12000 spots from the 9 analyzed fractions of 3 different patients. The range of the 3 treatment fields is very similar. The position of the Gaussian mean μ of each distribution is highlighted by a vertical dotted line, which serves as measure for the accuracy of range prediction.

Conclusion

The accuracy of PGI-based range verification was improved to enable the worldwide first in-man validation of CT-based stopping-power prediction. The evaluation of the first clinical PGI data for prostate-cancer treatments, systematically acquired within a clinical study, confirms the superiority of DECT-based range prediction in patients.

OC-0699 Relative biological effectiveness in proton therapy: accounting for variability and uncertainties

J. Ödén[1,2], K. Eriksson[2], E. Traneus[2], A. Dasu[3], P. Witt Nyström[3,4], I. Toma-Dasu[1,5]

[1]Stockholm University, Medical Radiation Physics, Stockholm, Sweden ; [2]RaySearch Laboratories AB, Research, Stockholm, Sweden ; [3]The Skandion Clinic, Radiation Oncology, Uppsala, Sweden ; [4]Danish Centre for Particle Therapy, Radiation Oncology, Aarhus, Denmark ; [5]Karolinska Institutet, Department of Oncology and Pathology, Stockholm, Sweden

Purpose or Objective

The increased relative biological effectiveness (RBE) at the end of the proton range might increase the risk of radiation-induced toxicities. This, however, is not accounted for in clinical practice when using the constant RBE of 1.1. This study aims to quantify the impact of variable RBE models with uncertainties in the plan evaluation and to apply indirect RBE optimisation for mitigating the potential clinical consequences.

Material and Methods

Proton plans with various fractionation doses for breast, brain, H&N and prostate cases (optimised with RBE=1.1) were evaluated using several LET_d- and α/ß-dependent RBE models. Resulting distributions of the RBE-weighted dose (D_{RBE}) and LET_d were analysed together with NTCPs. Furthermore, robustness evaluations accounting for uncertainties in setup, density, RBE model parameters, LET_d and α/ß were performed. Subsequently, two indirect RBE optimization methods were applied: (1) Re-optimising the physical dose based on variable RBE predictions from the LET_d distribution (LET_d-based re-optimisation). (2) Reducing the D_{RBE} in OARs while maintaining the physical target dose by penalising protons stopping in OARs (proton track-end optimisation). Reducing the number of track-ends is an appropriate surrogate for LET_d and RBE reduction, as both increase rapidly at the end of range.

Results

For CTVs with α/ß≈5-15 Gy, the D_{RBE} using variable RBE models was predicted to be similar to RBE=1.1 (average RBE of 1.05–1.15 for brain/H&N), whereas it was predicted to be higher for targets with α/ß≈1-5 Gy (average RBE of 1.1–1.3 for breast/prostate). For most OARs, the predicted D_{RBE} was often substantially higher, resulting in higher NTCPs. Inclusion of RBE uncertainties generally broadened the error bands for the nominal DVHs, with the largest contribution from the α/ß uncertainty. The LET_d-based re-optimisation allowed for satisfying target coverage for several variable RBE models and treatment sites. For prostate and breast cases, robust plans fulfilling clinical target and OAR goals were generated. Proton track-end optimisation allowed for substantial reductions in D_{RBE}, LET_d, and NTCP for several OARs compared to only dose-based optimisation, without compromising target coverage or the integral dose. For brain lesions, LET_d reduction of 50% or more could be achieved, resulting in fulfilment of clinical OAR goals assuming variable RBE models where dose optimised plans failed.

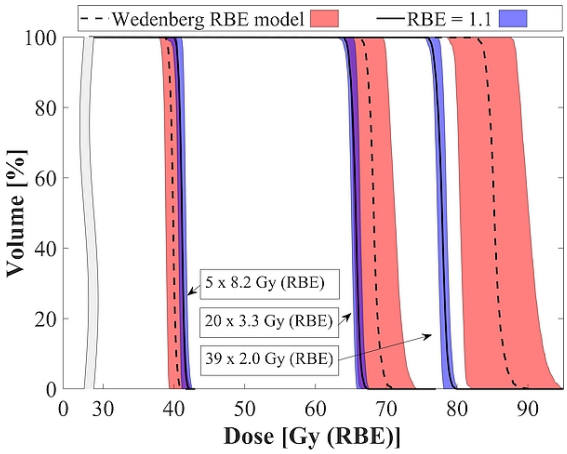

Fig. 1. DVHs with estimated error bands from the robustness evaluation of a prostate CTV using the constant RBE of 1.1 and a variable RBE model (Wedenberg et al. *Acta Oncol* 2013:52;580-5888) for three isoeffective fractionation schedules (α/β=5 Gy). The nominal DVHs for RBE=1.1 (solid lines) and for the Wedenberg RBE model (dashed lines) are shown together with their corresponding error bands. Setup and density uncertainties are included for RBE=1.1, whereas setup, range and RBE uncertainties (LET_d, model parameter and α/β) are included for the Wedenberg RBE model.

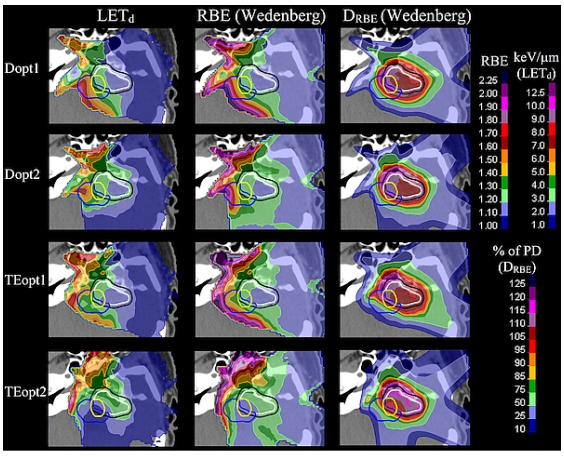

Fig. 2. Distributions of LET_d, RBE and RBE-weighted dose (D_{RBE}) using a variable RBE model (Wedenberg et al. *Acta Oncol* 2013:52;580-588) for a intracranial case with suspected radiation-induced brainstem necrosis. Two dose optimised plans (Dopt) and two proton track-end optimised plans (TEopt) are shown. Dopt1 (the clinical plan) and TEopt1 have two beams, whereas Dopt2 and TEopt2 have three beams. The delineations of CTV (white), PTV (black), brainstem (blue), and the MRI-delineated brainstem necrosis (yellow) are shown. Note the reductions in LET_d, RBE and D_{RBE} in the brainstem for TEopt2 compared to the other plans.

Conclusion

Robustness evaluation including RBE uncertainties allows for comprehensive analyses where potential adverse effects could be evaluated and mitigated on quantitative individual bases. LET_d-based re-optimisation could be used as a pragmatic solution for prostate and breast cases to fulfil clinical goals assuming variable RBE models, whereas proton track-end optimisation might be a generalised indirect RBE optimisation tool that could produce biologically advantageous plans compared to dose-optimised plans, without compromising physical criteria in current treatment protocols.

OC-0700 Accelerated robust IMPT optimization with sleeper scenarios

G. Buti[1], K. Souris[1], A. Barragan Montero[1], J.A. Lee[1], E. Sterpin[2]
[1]Université Catholique de Louvain, Molecular Imaging-Radiotherapy & Oncology, Brussels, Belgium ; [2]Katholieke Universiteit Leuven, Laboratory of Experimental Radiotherapy, Leuven, Belgium

Purpose or Objective

Robust optimization has shown to be essential in order to ensure an acceptable level of robustness in IMPT treatment plans (especially for lung tumor cases). However, the inherently excessive computational burden of the algorithm limits its use in the clinical environment. In this study, we propose an approximate worst-case robust optimization algorithm that significantly accelerates the optimization process, without compromising plan quality.

Material and Methods

Uncertainties due to setup errors, range errors and respiratory motion (characterized by a 4D-CT) are considered. In conventional worst-case robust optimization, the effects of the above-mentioned uncertainties are usually modeled by simulating a set of 63 scenarios (= 7 setup error scenarios x 3 range error scenarios x 3 breathing phases), and evaluating their corresponding dose at each iteration during optimization. The proposed method differs from conventional robust optimization by decomposing the original scenario set into (1) a dynamically updated 'active pool' of 10 candidate-worst scenarios and (2) a 'dead pool' that contains the 53 left-over scenarios. Because only the scenarios in the active pool are evaluated, a significant gain of optimization time is expected. The active pool scenarios are selected using a hidden probability vector P, which associates with each scenario, at all times, a 'worst-case probability'. P is updated at each iteration as follows: (1) the probability of the worst-case scenario is incremented, (2) the probabilities of the dead scenarios are incremented (giving them the possibility to contribute later on in the optimization) and (3) P is normalized so that the sum of all elements in P is 1 (effectively decrementing the probabilities of active scenarios which are currently not the worst-case). At all times, the 10 scenarios with the highest probabilities are selected in the active pool. The proposed method was implemented in the open-source robust optimizer MIROpt and tested for a 4D lung tumor patient (prescription of 60 Gy). The resulting treatment plan was benchmarked to a plan obtained from conventional worst-case robust optimization (using 63 scenarios). Treatment plans were evaluated by performing robustness tests (simulating breathing motion, setup and range errors) using the open-source Monte-Carlo dose engine MCsquare.

Results

An 80% reduction of plan optimization time is achieved by the proposed method. In terms of plan quality (see figure), the proposed method and conventional method perform similarly: both achieve a worst-case D95 of 58.5 Gy. Moreover, the difference in normal tissue sparing is also comparable (the difference in lung Dmean is only 0.5 Gy).

Conclusion

An approximate worst-case robust optimization method is proposed that achieves an optimization time gain of 80%, for the patient considered in this study, with similar performance compared to conventional worst-case robust optimization.